Modes of faulting at mid-ocean ridges

W. Roger Buck[1], Luc L. Lavier[2]* & Alexei N. B. Poliakov[3]

[1]*Lamont-Doherty Earth Observatory of Columbia University, Palisades, New York 10964, USA*
[2]*Seismological Laboratory, California Institute of Technology, Pasadena, California 91125, USA*
[3]*Royal Bank of Canada, 71 Queen Victoria Street, London EC4V 4DE, UK*

* Present address: Institute for Geophysics, Jackson School of Geosciences, University of Texas at Austin, 4412 Spicewood Springs Road, #600, Austin, Texas 78759-8500, USA

Abyssal-hill-bounding faults that pervade the oceanic crust are the most common tectonic feature on the surface of the Earth. The recognition that these faults form at plate spreading centres came with the plate tectonic revolution. Recent observations reveal a large range of fault sizes and orientations; numerical models of plate separation, dyke intrusion and faulting require at least two distinct mechanisms of fault formation at ridges to explain these observations. Plate unbending with distance from the top of an axial high reproduces the observed dip directions and offsets of faults formed at fast-spreading centres. Conversely, plate stretching, with differing amounts of constant-rate magmatic dyke intrusion, can explain the great variety of fault offset seen at slow-spreading ridges. Very-large-offset normal faults only form when about half the plate separation at a ridge is accommodated by dyke intrusion.

Faults are quasi-planar weak zones in the lithosphere, the brittle outer shell of the Earth, where earthquakes and tectonic strain are concentrated. To study how faults form it is logical to look at mid-ocean ridges, where faults are constantly forming. It is also particularly important to understand ridge fault systems because they affect major hydrothermal mineral deposits[1] and chemosynthetic biological communities[2].

A rift valley flanked by normal faults was the first feature identified as marking the axis of mid-ocean ridges when ridges were discovered 50 years ago[3]. To explain the 1–2-km-deep, 20–30-km-wide axial valley seen at most slow-spreading ridges (see Fig. 1b, c) was a great challenge of early ridge studies. A consensus emerged that stretching the cold brittle lithosphere at a ridge is what produces a valley[4,5,6].

The space generated at the valley by the far-field pull of plate tectonics can be filled by magmatic dyke intrusion at lower stress than is needed for faults to slip and accommodate tension[7]. For this reason, many authors assume that faults form only during periods when no magma is available for dyke intrusion and that the total slip on faults depends on the time interval between dyking events[8]. According to this standard model, all faults at ridges result from tectonic stretching of thin axial lithosphere during amagmatic periods[9].

In the last decade it has become clear that the stretching model cannot explain the variety of faults seen at ridges. Three specific observations stand out. First, the dip directions of mid-ocean-ridge normal faults show systematic variability as a function of spreading rate. Nearly all faults mapped at slow-spreading centres dip towards the axis, but about half of faults near fast-spreading centres dip towards the axis and the other half dip away[9]. Stretching faults should dip towards the axis.

Second, faults bounding abyssal hills near fast-spreading ridges begin to form ~2–4 km from the axis of normal axial highs[10] and not at the axis, where the seismically imaged lithosphere is thinnest[11–13]. Lavas cover faults offset very close to the axis[14], but abyssal-hill-bounding faults continue to grow out to 20–30 km from the axis[15].

Third, a completely different type of fault structure was discovered on parts of slow-spreading ridges called 'oceanic core complexes' or 'megamullion' structures[16–19] (Fig. 1c). Rather than pillow basalts that are cut by high-angle faults, the core complex surface, sometimes called a detachment, may expose gabbros and mantle rocks that were probably brought up from depths of at least several kilometres. These regions have been likened to continental metamorphic core complexes where rocks from depths of ~10 km are exposed at the surface. Oceanic core complexes occur mainly at the inside corners of ridge-transform intersections of slow-spreading ridges. The lithosphere of the outside corners looks more like typical slow-spreading lithosphere with moderate-amplitude abyssal hills and nearly continuous exposures of pillow basalts at the surface[20]. To fit these core complex structures into the standard stretching model, amagmatic spreading with durations of the order of a million years would be needed. Further, the standard model cannot explain the across-ridge asymmetry associated with most oceanic core complexes.

Faults at buoyancy-dominated ridges

Here we develop models of ridge axis deformation in the light of these observations. To deal with faulting at fast-spreading ridges we consider the effect of local buoyancy. Local buoyancy refers to lateral density variation on the scale of the axial region (within ~10 km of the axis). These density variations may be important at fast-spreading ridges because the axial lithosphere is very thin, hot and underlain by partially molten crust[11,12]. A few kilometres from a fast-spreading axis the lithosphere may be five times thicker than it is on axis and the crust may be solid[13,21]. The near-off-axis lithospheric thickness of both fast- and slow-spreading ridges may be nearly the same, on the basis of seismic interpretations and thermal models of ridges[22,23]. However, at slow-spreading ridges there may be much smaller differences between on- and off-axis lithospheric thickness[24] (see Fig. 2).

Lateral density variations may relate to the formation of the axial high seen at many fast-spreading centres (Fig. 1a). We adopt the approach of the recently developed accretional curvature model[25,26]. Unlike other models[27,28] it does not depend on potentially complex viscous flow under the ridge axis. Also, this model predicts a magnitude and distribution of brittle strain that is consistent with the average observed horizontal fault strain[25]. Previous numerical treatments of this model[26] could not resolve faults and so direct comparisons with observed fault populations have not been possible.

The main simplifying assumption in the model is that fluid magma rises to the level of local isostatic equilibrium at the axis of plate spreading. Local magmatic isostasy at the axis should occur when there is enough magma to accommodate all plate separation. A justification for this assumption comes from seismic results that show a bright reflector at a depth of 0.7–2 km along the axis of most ridges with axial highs[11,29]. This bright reflector has characteristics

consistent with a magma-filled lens and so is described as an axial magma chamber. Outside this region that is underlain by magma the lithosphere is too strong to respond in a local isostatic manner. The magma and underlying partial melt should accrete to the sides of the adjacent separating plates and get denser as it cools and freezes. This load bends down each plate, and additional accretion forms a plate with a concave upward curvature. As the curved plate passively moves away from the axis it unbends.

To look at fault development near ridges we use a numerical technique that allows for localization of the deformation in a brittle-plastic layer in shear zones simulating faults[6]. Faults are not specified but develop where the stress is sufficient for brittle yielding. The model uses an explicit finite-element approach that efficiently deals with elastic, viscous and brittle-plastic deformation and is set up in a way similar to our previous ridge faulting studies[6,30]. Because the buoyancy-dominated (or axial high) case is expected to develop symmetrically, only one side of the ridge is modelled. Magmatic accretion is assumed to account for all plate separation, so no stretching occurs at the axis. Dykes accrete by addition of a column of new elements at the axis every time the off-axis boundary has moved one grid spacing. The top of the new column is set to be at the level of local isostatic equilibrium. To simulate the freezing of partially molten lower crust, elements are also accreted at the non-vertical boundary between the weak axial zone and the brittle lithosphere (Fig. 2a). Deformation occurs because accreted elements are denser than the material in the axial partial melt zone. The density of the axial zone controls the normal stress boundary condition applied to the axial elements and to the level of accretion of the top accreted elements.

For a reasonable density contrast and brittle layer thicknesses the model reproduces both the shape of the axial high and some of the basic characteristics of the flanking faults. As shown in Fig. 3, the fully two-dimensional model fits the general shape of a real axial high. As with previous thin-plate models, the wavelength of the high depends on the off-axis plate thickness and a good fit was found for a 5-km-thick brittle plate. During plate unbending, extensional plastic failure, normal fault nucleation and offset would occur in the top of the plate above a neutral depth—with compressional failure below that depth.

The pattern of faulting in the numerical models of axial-high-related plate unbending is very sensitive to the prescribed rate and amount of weakening with strain. If the rate of strain weakening is low, say 10 MPa of strength loss over a strain of 50%, then no localization into fault-like behaviour is seen. In contrast, for a high rate and large amount of strain weakening, curved faults developed that cut completely through the lithosphere. Bending was concentrated on these widely spaced 'hinge' faults, but did not result in appreciable fault-offset-related surface relief.

Only with limited strength loss that occurred very rapidly with strain does the model develop a fault pattern that bears some resemblance to real axial-high flanking faults. As shown in Fig. 3, a good case had 10 MPa of cohesion loss occurring over 1% of strain. After a phase of fast-strain weakening, continued slow-strain weakening does not affect the bending faults because bending strains are small. Pairs of graben-bounding faults that dipped towards each other developed during plate unbending. The faults did not develop appreciable offset until they were several kilometres away from the axis and they grew steadily out to a

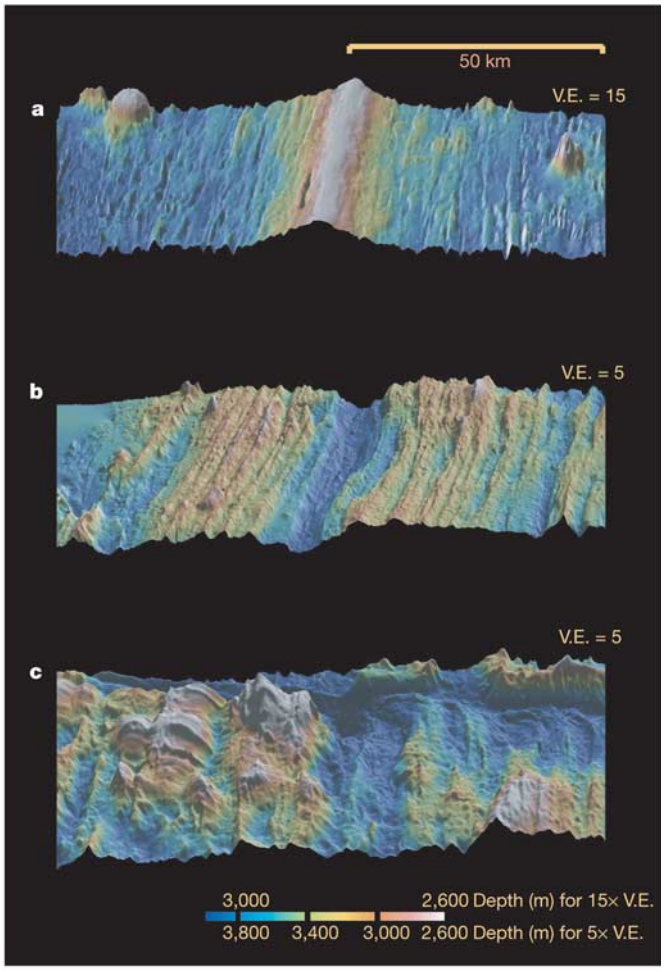

Figure 1 Shaded relief images of bathymetry over three contrasting sections of the mid-ocean ridge system. Each image shows ~40 km along the ridge axis and ~110 km across the axis. The vertical exaggeration (V.E.) is three times greater for the top image than for the other two. **a**, Relief across the axial high at 9° 37′ N latitude on the East Pacific Rise showing the small (~50 m) relief of the abyssal hills that parallel the axis. **b**, Much larger abyssal hills are seen parallel to the axial valley along the 115° E longitude segment of the intermediate spreading rate Southeast Indian Ridge. **c**, The intersection of the Mid-Atlantic Ridge, along the centre of image, with the nearly east–west trending Kane transform and fracture zone (on the left and right sides at the top of the image). The image, centred at 23° 25′ N latitude, shows that the east side of the ridge has abyssal hills parallel to the axis, as in **b**. Starting ~20 km west of the axis is a ~15-km-wide, 30-km-long structure with great topographic relief and with shorter wavelength 'corrugations' striking perpendicular to the ridge. Profiles orthogonal to these ridge segments, going through the centres of the images, are shown in Figs 3 and 5. Images made with GeoMapApp[39] software with multibeam sonar data[40–42].

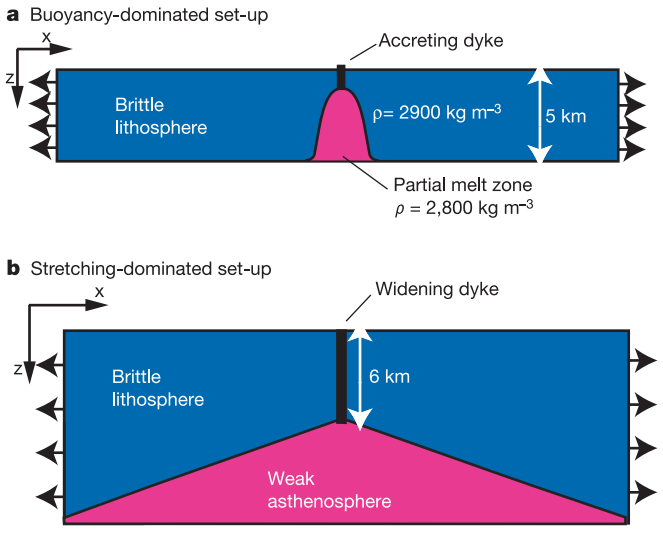

Figure 2 Set-up for numerical models. **a**, Structure used to model a ridge where near-axis buoyancy variations control the topographic relief and faulting. **b**, Set-up for stretching-dominated ridge with a fixed temperature structure.

distance of ~20–25 km. The faults develop over such a wide distance range because that is where progressive unbending occurs, and the faults cease growing where the plates are essentially flattened out. A maximum fault-related relief of >50 m was developed in the models, in the range of observed values[9].

Faults at stretching-dominated ridges

To deal with the apparent variety of stretching-related faulting we consider that ridge-axis dyke intrusion at various rates must be considered. Real dykes are intruded over a matter of days with the time between intrusion events measured in years[31], but in the model we consider the time-averaged rate of dyke intrusion. Magmatic accretion is assumed to occur at a constant rate at all depths through the axial lithosphere. The rate of dyke opening is specified by the fraction of the plate separation rate, M, that is accommodated by magmatic dyke opening. For $M = 0$, dykes account for none of the plate spreading and for $M = 1$, dykes accommodate all the plate separation.

Dykes are assumed to open at one horizontal position in a cross-section of a ridge axis. This assumption is based on the idea of feeding of melt to magma chambers at the centres of ridge segments, for which there is ample evidence[31,32]. Dykes supplied from a central magma chamber have to open in nearly straight lines to keep the supply of magma flowing along and into an opening dyke. Dyke intrusion may supply much of the heat that keeps the axis hotter and the axial lithosphere thinner than the lithosphere farther from the axis. Solid-state advection below the ridge axis should also affect the thermal structure of the ridge axis, but for simplicity we fix the thermal structure.

A simple geometric argument shows how faults and dykes might interact at a ridge with a fixed position of dyking and fixed thermally defined strength structure. If one fault forms owing to lithospheric stretching then it should initially cut the thinnest axial lithosphere on one side of the axis, shown in Fig. 4. If the fault moves away from the axis into thicker lithosphere, it then becomes harder to continue offsetting that fault even though it is weaker than the surrounding lithosphere. Eventually, it will be easier to form a new fault cutting the axis and the first fault will be abandoned.

Insights from previous models of normal faulting[33] show that when a normal fault forms, one side moves up and away from the fault by about the same amount that the other side moves down and away from the fault. Eventually, the down-dropping side (the hanging-wall block) cannot drop further and stops deforming. The other (footwall) block continues to move up and out as asthenosphere from below accretes to that layer. Because the hanging-wall block no longer deforms, but continues to translate, the active part of the fault moves with the hanging wall. As a result, faults should move with the hanging-wall block, as inferred from these model results. As shown in Fig. 4, the plate to the left of the axis moves with velocity $-V_p/2$, where V_p is the total plate separation rate. The velocity step across the axial dyke is MV_p. Thus, the hanging-wall block of the fault will move away from the axis at a speed of $V_p(M - 0.5)$.

For $M = 0.5$ the hanging wall of the fault does not move away from the axis, so the fault could build up potentially unlimited offset. The distance L from the axis out to which the fault can remain active should depend on the strength structure of the axis and the fault-weakening parameters. The horizontal component of fault slip rate is $V_p(1 - M)$, so the amount of fault offset before abandonment is $L(1 - M)/(M - 0.5)$, as plotted in Fig. 4. For M close to 1 the maximum fault offset can be small, while for M close to 0.5 the offset should be very large compared to L. This plot is at best a qualitative guide to expected results because L is expected to be a nonlinear function of fault offset[33,34].

A numerical model of dyking and stretching

To look at fault development we treat the model of stretching and dyking using the same numerical technique used for the buoyancy cases, except that we allow for asymmetric deformation across the axis. Dyke opening is simulated with a vertical column of special elasto-plastic dyke elements that are made to widen at a constant rate. The dyke column is placed at the axis of the assumed symmetric ridge thermal and strength structure (Fig. 2b). The top of the dyke is set at the height of the adjacent elements, which are free to move up or down in the course of a calculation. The base of the dyke column is placed within the weak asthenosphere, which always deforms via viscous creep (see Supplementary Information for details).

To approximate the strength structure of slow-spreading ridges we assumed uniform elastic coefficients, pressure- and strain-dependent Mohr Coulomb brittle-plastic failure stresses and temperature-dependent non-newtonian viscosity (Supplementary Information).

Several dozen numerical cases were run with various values of M, strain weakening rates and numerical grid sizes. The results of two cases with the same strength structure, grid size and strain-weakening parameters are shown in Fig. 5. These cases show that the normal fault offset varies greatly as a function of M and that for $M = 0.5$ we can get a very large fault offset, as predicted by our kinematic conceptual model. For $M = 0.95$, the model also generates a fairly symmetric pattern of mainly inward-dipping, small-offset faults, and a symmetric axial valley.

For $M = 0.5$ the model produced two large faults with offsets 20 to 30 km on one side of the spreading axis and a series of small faults on the other. On the opposite side of the axis, a series of small-offset normal faults develop, along which the lithosphere moves up from the deep axial valley region. We believe that these small faults, which were not part of our kinematic conceptual model, accommodate a small part of the tectonic stretching across the axis. This small stretching on one side of the axis will contribute to migration of the large-offset faults away from the axis on the other side of the axis. This may account for the limited offset of the large faults seen in this case.

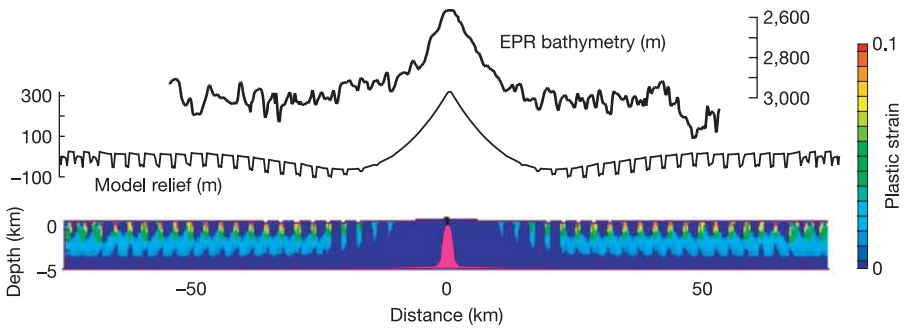

Figure 3 Results for buoyancy-dominated ridge models. The shape of the model axial high and the spacing and relief of the faults is similar to that observed at 9° 37′ N on the East Pacific Rise (from Fig. 1a). Half the bending faults dip towards the axis and half away, which is also consistent with observations.

Structures developed in association with model large-offset faults are similar to the oceanic core complexes seen at more than twenty ridge-transform intersections on slow-spreading ridges[17–19]. Besides having a similar range of relief for the axial valley and the inside-corner high (2 km), the model topography has other characteristics observed on topographic profiles for an ocean core complex (Fig. 5b): (1) a domed shape with a flat-lying abandoned-fault footwall; and (2) the characteristic shape of the fault breakaway. Also, for $M = \sim 0.5$ nearly all the magmatic accretion occurs on the side of the axis with small-offset faults, as may happen at outside corners of some ridge-transform intersections. Finally, although it is not well resolved in our numerical models, the bending associated with large fault offsets should result in small-offset, high-angle faults. Such distributed small-offset, high-angle normal faults are seen on the surface of oceanic core complexes[18,19].

To get the large-offset faults that may characterize oceanic core complexes our models require that three conditions be met. First, M has to be close to 0.5. Next, the fault weakening must be large and more than half of the weakening has to occur moderately slowly with strain. Finally, the lithosphere cannot thicken very fast with distance from the axis.

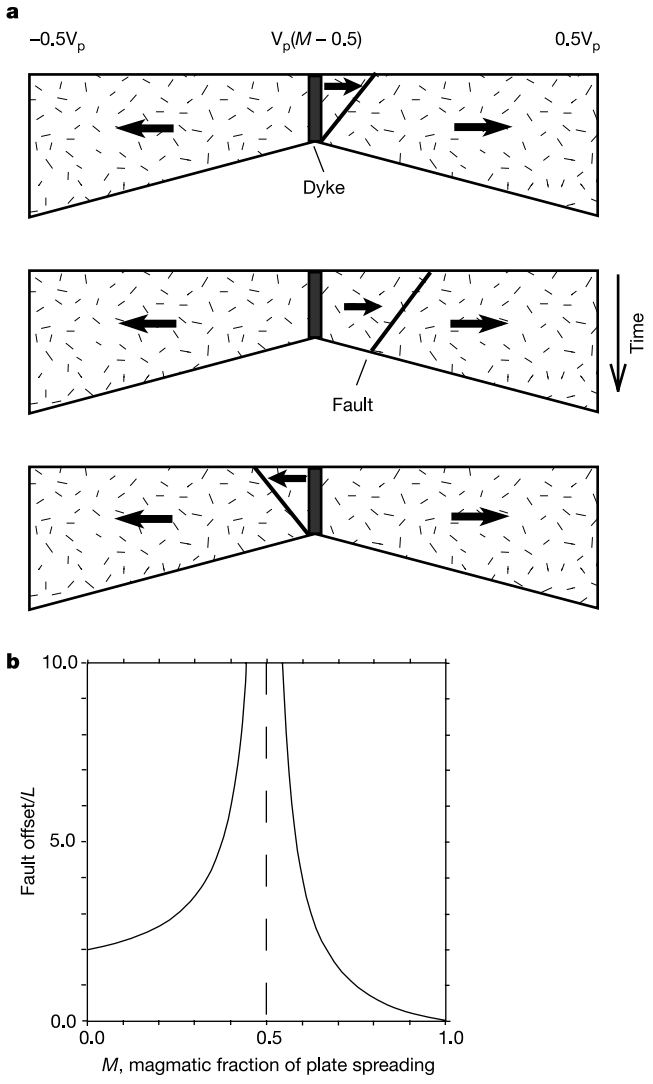

Figure 4 Illustration of kinematic stretching fault model. **a**, Cartoon showing how the hanging-wall block of a fault may migrate during ridge stretching as a function of the fraction, M, of plate separation accommodated by magmatic dyke opening. The velocity of the hanging-wall block relative to the axis is $V_p(M - 0.5)$, where V_p is the full spreading rate. The position of the hanging-wall block should control the fault location. For $M > 0.5$ the hanging wall moves away from the axis, but for $M = 0.5$ the hanging wall does not move laterally with time. **b**, Plot of estimated fault offset as a function of M for the kinematic stretching and dyking ridge model. L is the maximum off-axis distance of fault activity.

Magma supply and fault mode

A single set of fault strain-weakening parameters reproduced the essential features of both stretching- and bending-related faults. Two phases of strain weakening were needed. Nearly instantaneous strength reduction had to occur, once the yield stress was reached, for bending to produce small-offset, inward- and outward-dipping faults similar to those seen near axial highs. Slower strain weakening had to occur to get larger-offset faults seen at some slow-spreading centres. For both the buoyancy- and stretching-dominated model cases the same strain-weakening parameters were used: with fast weakening for the first percent of strain and slow strain weakening for greater strain. The fast strain weakening may correspond to the sudden loss of cohesion as a fault break forms. The continued weakening may relate to wearing and widening of the fault zone with greater offset. It is possible that these strain-weakening parameters may also describe how faults form in other tectonic environments, such as strike–slip and thrust-faulted regions.

The numerical models developed here show how distant loads and local loads may produce very different modes of normal faulting at mid-ocean ridges. All loads driving plate motion and deformation are produced by lateral density variations in the Earth. Stretching is related to loads and motions at the scale of plate tectonics. The tectonic pull caused by cooling and contraction of plates that float on a weak asthenosphere can contribute to stretching by transmitting stresses over long distances. Local loads, related to magmatic accretion and near-axis cooling, may drive

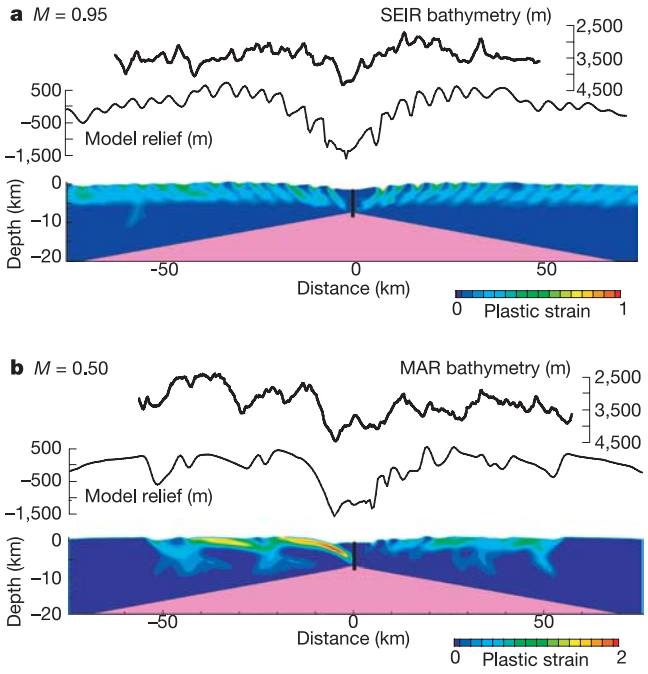

Figure 5 Results for stretching-dominated ridge models. Two model cases are shown in **a** and **b** for different values of M, but with the same lithospheric structure. **a**, Note the fairly symmetric axial valley and the moderate fault offsets for $M = 0.95$ which matches the sense of the bathymetric profile from the 115° E segment of the Southeast Indian Ridge (from Fig. 1b). Reducing the model lithospheric thickness by about one-third produces a better fit to this bathymetry. **b**, Faults with very large offset occur for $M = 0.5$. The model topographic profile is similar to that observed near the intersection of the Mid-Atlantic Ridge and the Kane transform (from Fig. 1c). The model is consistent with the large offset faults seen at the inside corners of such slow-spreading segments, as well as with the asymmetry in magmatic accretion, because most magmatic accretion takes place on the side of the ridge with smaller fault offsets.

lithospheric bending and faulting at any ridge. Bending-related faulting is the dominant faulting mode at fast- and perhaps at some intermediate-spreading centres.

The pattern of faulting produced by stretching a spreading centre is controlled by the rate of magmatic accretion. Temporal variations in magma supply on a very long timescale are not required to produce large-offset faults. The across-axis strength structure can also affect the pattern of faulting, although the models presented here do not deal with different strength structures. For M less than 1, the thermal advection related to fault offset may affect the ways faults continue to slip, but this is a complex question related to hydrothermal cooling of lithosphere[35].

We have considered only end-member cases to demonstrate these ideas, so we can only speculate about the behaviours of ridge segments with a range of spreading rates and magma supply. Many intermediate-spreading ridge segments fit reasonably well into our end-member categories, some being buoyancy-dominated and some stretching-dominated. At the slowest-spreading ridges, sometimes called ultraslow-spreading ridges[36], an extreme range of along-axis variations in magma abundance is seen on a segment scale ($\sim$100 km)[36,37,38]. Unlike typical spreading segments, magma-starved parts of ultraslow-spreading segments can be oblique to the spreading direction. The obliquity of nearly amagmatic parts of ultraslow-spreading ridges may be directly tied to the lack of dyke intrusions coming from a magma chamber at the centre of a segment.

In these models, even small-magnitude stretching (that is M just less than 1) produces large axial valley relief. Maximum relief increases with increasing model axial lithospheric thickness, on the basis of models not presented here. Increased axial valley relief seen at slow-spreading segment ends compared to segment centres correlates with thicker lithosphere at the ends than at centres[24].

If our view of the kinematics of the hanging-wall block bounded by a fault and an axial dyke (Fig. 4) for $M \approx 0.5$ is correct, then it suggests a simple explanation for oceanic core complex formation on the inside corner of a ridge-transform intersection. Having this block on the inside of the ridge-transform intersection minimizes the shear strain across the transform. An outside-corner core complex would require slip on the extension of the transform outside the ridge-transform intersection.

The great variations in the fault pattern along many 'normal' slow-spreading segments (for example, Fig. 1) appear to require very different rates of magmatic dyke intrusion along those segments. There may be a central, magma-rich part of these segments where the magma supply is nearly enough to accommodate plate separation (M just below 1) with an adjacent magma-poor part of the segment where $M \approx 0.5$. Our work shows that differences in magmatic input to dykes may produce the observed differences in faults. Understanding why the magmatic accommodation of plate separation varies so much along ridge segments, and why it seems to occur in various modes rather than vary smoothly, is a clear challenge to understanding how spreading centres work. □

Received 8 September 2004; accepted 12 January 2005; doi:10.1038/nature03358.

1. Hannington, M. D., Jonasson, I. R., Herzig, P. M. & Petersen, S. in *Seafloor Hydrothermal Systems; Physical, Chemical, Biological, and Geological Interactions* (eds Humphris, S. E., Zierenberg, R. A., Mullineaux, L. S. & Thomson, R. E.) 115–157 (American Geophysical Union, Washington DC, 1995).
2. Van Dover, C. L. Evolution and biogeography of deep-sea vent and seep invertebrates. *Science* **295,** 1253–1257 (2002).
3. Heezen, B. C. The rift in the ocean floor. *Sci. Am.* **203,** 99–106 (1960).
4. Tapponnier, P. & Francheteau, J. Necking of the lithosphere and the mechanics of slowly accreting plate boundaries. *J. Geophys. Res.* **83,** 3955–3970 (1978).
5. Lin, J. & Parmentier, E. M. A finite amplitude necking model of rifting in brittle lithosphere. *J. Geophys. Res.* **95,** 4909–4923 (1990).
6. Poliakov, A. N. B. & Buck, W. R. in *Faulting and Magmatism at Mid-Ocean Ridges* (eds Buck, W. R., Delaney, P. T., Karson, J. A. & Lagabrielle, Y.) 305–324 (American Geophysical Union, Washington DC, 1998).
7. Price, N. J. & Cosgrove, J. W. *Analysis of Geological Structures* 1–452 (Cambridge Univ. Press, Cambridge, UK, 1990).
8. Thatcher, W. & Hill, D. P. A simple model for fault generated morphology of slow-spreading mid-oceanic ridges. *J. Geophys. Res.* **100,** 561–570 (1995).
9. Carbotte, S. M. & Macdonald, K. C. Causes of variation in fault-facing direction on the ocean floor. *Geology* **18,** 749–752 (1990).
10. Macdonald, K. C., Fox, P. J., Alexander, R. T., Pockalny, R. & Gente, P. Volcanic growth faults and the origin of the Pacific abyssal hills. *Nature* **380,** 125–129 (1996).
11. Detrick, R. S. *et al.* Multichannel seismic imaging of the crustal magma chamber along the East Pacific Rise. *Nature* **326,** 35–41 (1987).
12. Vera, E. E. *et al.* The structure of 0- to 0.2-m.y.-old oceanic crust at 9°N on the East Pacific Rise from expanded spread profiles. *J. Geophys. Res.* **95,** 15529–15556 (1990).
13. Dunn, R. A. *et al.* Three-dimensional seismic structure and physical properties of the crust and shallow mantle beneath the East Pacific Rise at 9N. *J. Geophys. Res.* **105,** 23537–23556 (2000).
14. Karson, J. A. *et al.* Structure of the uppermost fast-spread oceanic crust exposed at the Hess deep: Implications for subaxial processes at the East Pacific Rise. *Geochem. Geophys. Geosyst.* **2,** 1002, doi:10.1029/2001GC000155 (2001).
15. Alexander, R. T. & Macdonald, K. C. Sea Beam, Sea MARC II and ALVIN based studies of faulting on the East Pacific Rise 9°20′ N-9°50′ N. *Mar. Geophys. Res.* **18,** 557–587 (1996).
16. Karson, J. A. *et al.* Along-axis variations in seafloor spreading in the MARK area. *Nature* **328,** 681–685 (1987).
17. Cann, J. R. *et al.* Corrugated slip surfaces formed at ridge-transform intersections on the Mid-Atlantic Ridge. *Nature* **385,** 329–332 (1997).
18. Tucholke, B. E., Lin, J. & Kleinrock, M. Megamullions and mullion structure defining oceanic metamorphic core complexes on the Mid-Atlantic Ridge. *J. Geophys. Res.* **103,** 9857–9866 (1998).
19. Blackman, D. K. *et al.* Geology of the Atlantis Massif (MAR 30°N): Implications for the evolution of an ultramafic core complex. *Mar. Geophys. Res.* **23,** 443–469 (2004).
20. Tucholke, B. E. & Lin, J. A geologic model for the structure of ridge segments in slow-spreading ocean crust. *J. Geophys. Res.* **99,** 11937–11958 (1994).
21. Crawford, W. C., Webb, S. C. & Hildebrand, J. A. Estimation of shear velocities in the oceanic crust from compliance measurements by two-dimensional finite difference modeling. *J. Geophys. Res.* **103,** 9895–9916 (1998).
22. Purdy, G. M., Kong, L. S. L., Christeson, G. L. & Solomon, S. C. Relationship between spreading rate and the seismic structure of mid-ocean ridges. *Nature* **355,** 815–817 (1992).
23. Phipps Morgan, J. & Chen, Y. J. The genesis of oceanic crust: magma injection, hydrothermal circulation and crustal flow. *J. Geophys. Res.* **98,** 6283–6297 (1993).
24. Barclay, A. H., Toomey, D. R. & Solomon, S. C. Microearthquake characteristics and crustal V_P/V_S structure at the Mid-Atlantic Ridge, 35°N. *J. Geophys. Res.* **106,** 2017–2034 (2001).
25. Buck, W. R. Accretional curvature of lithosphere at magmatic spreading centers and the flexural support of axial highs. *J. Geophys. Res.* **106,** 3953–3960 (2001).
26. Shah, A. & Buck, W. R. Causes for axial high topography at mid-ocean ridges and the role of crustal thermal structure. *J. Geophys. Res.* **106,** 30865–30880 (2001).
27. Kuo, B. Y., Forsyth, D. W. & Parmentier, E. M. Flexure and thickening of the lithosphere at the East Pacific Rise. *Geophys. Res. Lett.* **13,** 681–684 (1986).
28. Eberle, M. A. & Forsyth, D. W. An alternative, dynamic model of the axial topographic high at fast spreading ridges. *J. Geophys. Res.* **103,** 12309–12320 (1998).
29. Hooft, E. E., Detrick, R. S. & Kent, G. M. Seismic structure and indicators of magma budget along the Southern East Pacific Rise. *J. Geophys. Res.* **102,** 27319–27340 (1997).
30. Buck, W. R. & Poliakov, A. N. B. Abyssal hills formed by stretching oceanic lithosphere. *Nature* **392,** 272–275 (1998).
31. Einarsson, P. & Brandsdottir, B. Seismological evidence for lateral magma intrusion during the July 1978 deflation of the Krafla volcano in NE-Iceland. *J. Geophys.* **47,** 160–165 (1980).
32. Magde, L. & Sparks, D. W. Three dimensional mantle upwelling, melt generation and melt migration beneath segmented slow spreading ridges. *J. Geophys. Res.* **102,** 20571–20583 (1997).
33. Lavier, L. L., Buck, W. R. & Poliakov, A. N. B. Factors controlling normal fault offset in an ideal brittle layer. *J. Geophys. Res.* **105,** 23431–23442 (2000).
34. Buck, W. R. Effect of lithospheric thickness on the formation of high- and low-angle normal faults. *Geology* **21,** 933–936 (1993).
35. Lavier, L. L. & Buck, W. R. Half graben versus large-offset low-angle normal fault: The importance of keeping cool during normal faulting. *J. Geophys. Res.* **107,** 10.1029/2001JB000513 (2002).
36. Dick, H. J. B., Lin, J. & Schouten, H. An ultraslow-spreading class of ocean ridge. *Nature* **426,** 405–412 (2003).
37. Cochran, J. R., Kurras, G. H., Edwards, M. H. & Coakley, B. J. The Gakkel Ridge: Bathymetry, gravity anomalies and crustal accretion at extremely slow spreading rates. *J. Geophys. Res.* **108,** doi:10.1029/2002JB001830 (2003).
38. Michael, P. J. *et al.* Magmatic and amagmatic seafloor generation at the ultraslow-spreading Gakkel Ridge, Arctic Ocean. *Nature* **423,** 956–961 (2003).
39. Haxby, W. *GeoMapApp version 1.2_02*; ⟨http://www.GeoMapApp.org/⟩ (Marine Geosciences Data Management System, downloaded August 2004).
40. Cochran, J. R. *et al.* The Southeast Indian Ridge between 88°E and 120°E: Gravity anomalies and crustal accretion at intermediate spreading rates. *J. Geophys. Res.* **102,** 15463–15487 (1997).
41. Macdonald, K. C. *et al.* The East Pacific Rise and its flanks, 8–18°N: History of segmentation, propagation and spreading direction based on SeaMARC II and SeaBeam studies. *Mar. Geophys. Res.* **14,** 299–344 (1992).
42. Gente, P. *et al.* Characteristics and evolution of the segmentation of the Mid-Atlantic Ridge between 20 degrees N and 24 degrees N during the last 10 million years. *Earth Planet. Sci. Lett.* **129,** 55–71 (1995).

Supplementary Information accompanies the paper on **www.nature.com/nature**.

Acknowledgements Work supported by the National Science Foundation. We thank W. Haxby for help with images and J. Karson for comments on the text.

Competing interests statement The authors declare that they have no competing financial interests.

Correspondence and requests for materials should be addressed to W.R.B. (buck@ldeo.columbia.edu).